



Energy and electron transfer reactions of polyenic acids with variable chain lengths



Asma Zaidi^{a,†}, He Li^{a,†}, Hans-Richard Sliwka^{a,*,†}, Vassilia Partali^{a,†}, Hansgeorg Ernst^b, Thor B. Melø^{c,*}

^a Department of Chemistry, Norwegian University of Science and Technology, 7491 Trondheim, Norway

^b BASF SE, Fine Chemical Research, 67056 Ludwigshafen, Germany

^c Department of Physics, Norwegian University of Science and Technology, 7491 Trondheim, Norway

ARTICLE INFO

Article history:

Received 12 June 2012

Received in revised form

25 September 2012

Accepted 15 October 2012

Available online 22 October 2012

Keywords:

Antioxidant

Carotenoids

Electron transfer

Energy transfer

Carboxylic acids

ABSTRACT

Highly unsaturated conjugated fatty acids (carotenoic acids) with 5–15 conjugated double bonds were irradiated by flash pulses in the presence of the sensitizer riboflavin. The resulting triplet and radical cation transients were analyzed and the underlying energy and electron transfer reactions determined experimentally and by calculation. The two key antioxidant reactions of carotenoids summarize in a_r , the ratio of the reaction constants for electron and energy transfer. The optimal antioxidant ratio a_r cumulated in the polyenic acid with 11 double bonds. The photophysical formation of radical cations was chemically ascertained by reaction of the acids with FeCl_3 .

© 2012 Elsevier Ltd. All rights reserved.

1. Introduction

The electron-rich carotenoids are eminent electron donors as well as distinguished triplet energy acceptors. The combination of these properties established the reputation of carotenoids as potent antioxidants. Antioxidation can be characterized (a) by electron transfer, i.e., the carotenoid delivers an electron to a molecule depreciated of electrons, or (b) by energy transfer, i.e., the carotenoid combats oxygen in its highly reactive singlet electron configuration taking over oxygen's excessive energy. Other possible antioxidant mechanisms operate to a minor degree with carotenoids (radical addition, H-transfer, chemical oxygen quenching) or occur with specific radicals ($\text{O}_2^{\cdot-}$).^{1–3} The antioxidant effect of carotenoids has been determined (a) by varying the peripherals (rings, substituents) keeping the polyene chain constant or (b) by keeping the peripherals constant varying the chain lengths.^{4,5} The first method ranked astaxanthin and dihydroxyisorenieratene as superior antioxidants;^{6,7} the result of the second method is not uniquely identified. However, it is commonly assumed the longer a polyene chain the better the antioxidant properties. On the other hand, systematic measurements with different carotenoids have suggested an optimal chain length

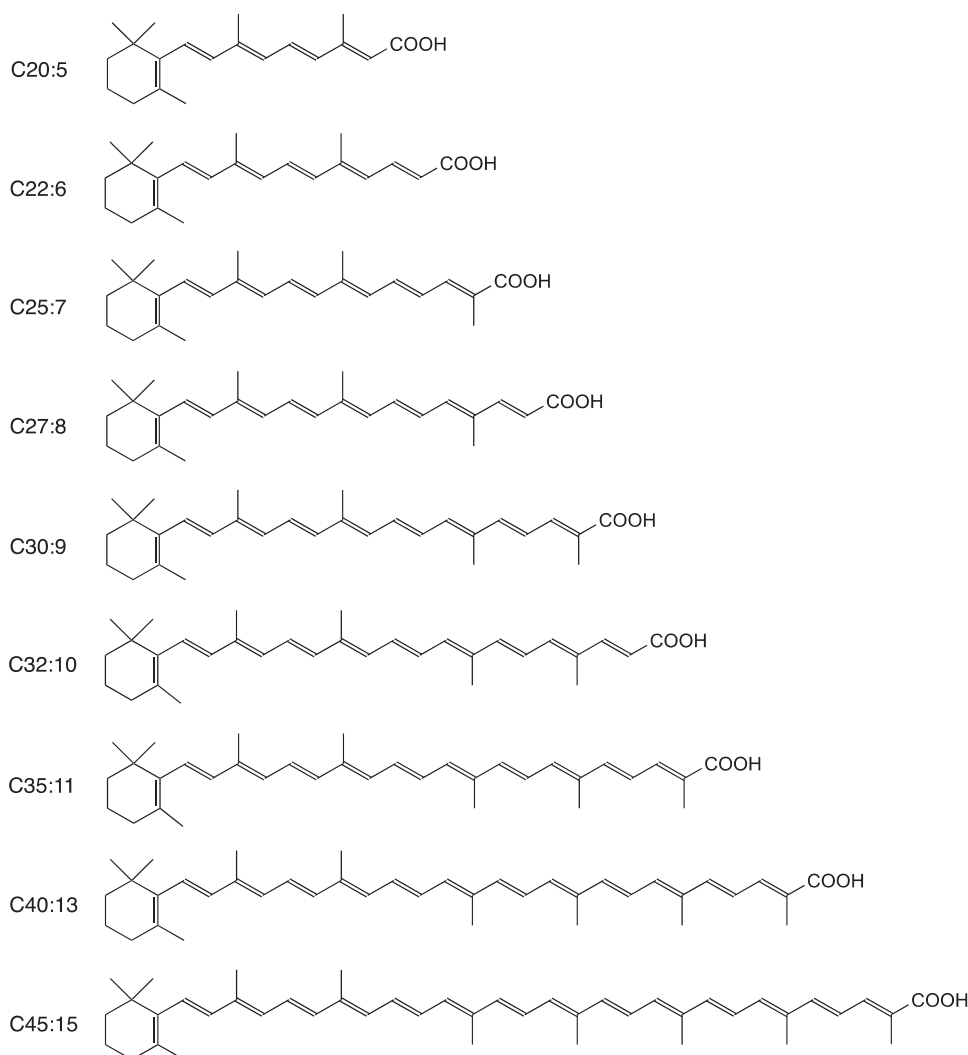
for diverse functions, e.g., 11 double bonds for singlet oxygen quenching, 7–11 or 9 and 11 double bonds for photobleaching protection, 10 or 9–11 double bonds for light harvesting function, and 7 double bonds for photon-to-current conversion (solar cell).^{8–14}

Since an all-purpose method for determining the total antioxidant activity (TAA),¹⁵ total antioxidant capacity (TAC),¹⁶ or total antioxidant potential (TAP)¹⁷ is lacking the results depend above all on the test system.¹⁸ The common antioxidant acronyms largely ignore carotenoids as a singlet oxygen quencher (energy transfer reaction).¹⁹ Our own antioxidant measurements showed to either energy or electron transfer but did not encompass both actions.^{20–25} A theoretical study with 28 miscellaneous carotenoids established the $^1\text{O}_2$ -quenching constant, the ionization energy and the HOMO–LUMO energy difference as distinct descriptors for the antioxidant property.²⁶ Another work concentrated only on electron transfer processes and related the antioxidant properties to the redox potentials.²⁷ We concentrated in this study on both the energy and electron transfer reaction of a series of carotenoic acids (Car) specified as C_n (n =number of carbon atoms) with N $\text{C}=\text{C}$ bonds $C_n:N$, i.e., $\text{C}_{20}:5$ – $\text{C}_{45}:15$. The compounds are interrelated; the only variable is the number of double bonds (Scheme 1).

Generally, Car do not easily react with other organic compounds. Therefore, Car are not affected by riboflavin (Rib), tocopherol (Toc), chlorophyll (Chl), nitronaphthalene (NN), or other sensitizers (Sen).^{20,28–30} However, when these sensitizers are irradiated, they

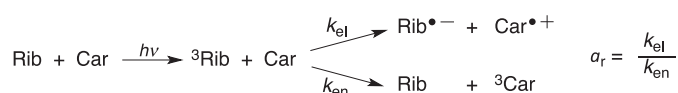
* Corresponding authors. E-mail addresses: hrr@nvg.ntnu.no (H.-R. Sliwka), thor.melo@ntnu.no (T.B. Melø).

† Fax: +47 73596155.



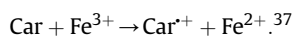
Scheme 1. Carotenoid acids (Car) specified as C_n (*n*=number of carbon atoms) with N C=C bonds: C_n:N. Particular names: C20:5 retinoic acid, C35:11 neurosporaxanthin, C40:13 torularhodin.

become excited to their high energetic triplet state, e.g., ³Rib, ³Toc, ³Chl, ³NN, ³Sen; these triplet species can now react with Car: Car releases either an electron to ³Rib developing the radical ions Car^{•+} and Rib^{•-} or the energy of ³Rib is transferred to Car forming ³Car (Scheme 2).³¹



Scheme 2. The predominant channels of carotenoid antioxidant reactions; *k*_{el} and *k*_{en} are the reaction constants for electron and energy transfer. The antioxidant ratio is expressed as *a*_r.

While the assignment of ³Car is unproblematic,³² the spectroscopic characterization of other Car transients is ambiguous. Carⁿ⁺, Car^{•+}, Carⁿ⁻, Carⁿ⁻ all appear in the same bathochromic wavelength region.^{33–36} For that reason, the photophysical generation of Car^{•+} was validated by chemically generated cation radicals:



We specifically examine in this work:

1. The absorption spectra of Car, ³Car and Car^{•+} relative to N
2. The energy and electron transfer rate constants *k*_{el} and *k*_{en}

3. The antioxidant ratio *a*_r=*k*_{el}/*k*_{en}
4. The optimal chain length for *a*_r

2. Results and discussion

Synthesis. Acids C20:5–C35:11 were produced by BASF.³⁸ C40:13 and C45:15 were synthesized by subsequent Wittig reactions from the relevant aldehyde precursors (Experimental section).

Absorption spectra. The broad absorption bands of the shorter acids resolve gradually into fine structural features with increasing chain length (Fig. 1). A similar spectroscopic pattern has been observed with other long chain carotenoids.^{39–41} The longer the conjugation the smaller is the increase in λ_{max} of Car and ³Car, whereas λ_{max} of Car^{•+} increased linearly with N (Fig. 2).

The development of chemically generated Car^{•+} was monitored visually (solutions turned to red, blue and black) and by VIS spectroscopy (Figs. 3 and 4, 1SD). Table 1 collects λ_{max} or 0←0 vibrational transitions (assigned by deconvolution of the experimental line shapes) for Car, ³Car and Car^{•+}. The values of λ_{max} largely agree for photophysically and chemically created Car^{•+} confirming the identity of the generated radical cations (Table 1).

The flash photolysis of the Rib/Car solution generated four species (Scheme 2, Fig. 12, Experimental section). Subtracting the spectra of ³Rib and Rib^{•-} from the spectrum of the compound mixture uncovered the neat spectra of ³Car and Car^{•+} as

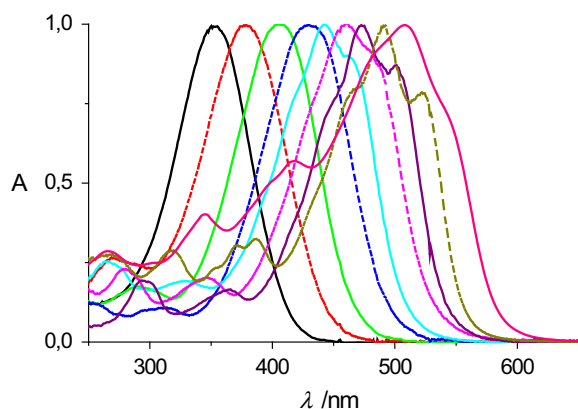


Fig. 1. UV-vis spectra of carotenoid acids C20 —, C22 ●●●●, C25 —, C27 ●●●●, C30 —, C32 ●●●●, C35 —, C40 ●●●● and C45 — dissolved in MeCN/H₂O=9:1. The spectra are normalized to unity at λ_{\max} for better comparison. Spectra of C27–C40 acids have been previously measured in petroleum ether.⁴²

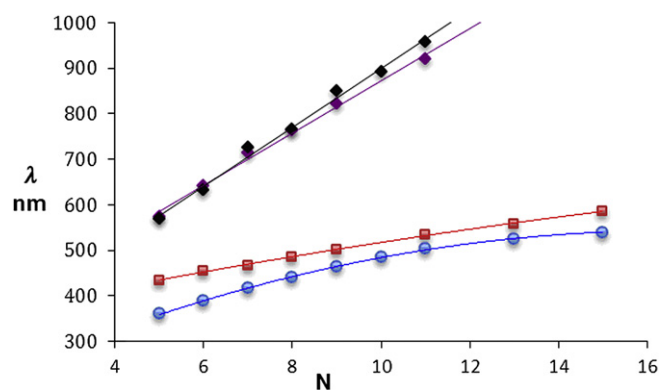


Fig. 2. Increase of λ_{\max} with the number of double bonds N. Car, ³Car, Car⁺ (light MeCN), Car⁺ (FeCl₃, CH₂Cl₂).

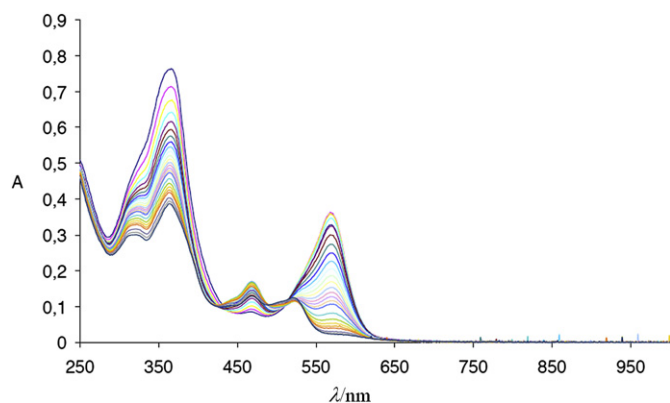


Fig. 3. Formation of C20⁺ (λ_{\max} =568 nm) with FeCl₃ in CH₂Cl₂. The decay of C20⁺ is accompanied with the growth of oxidation products at 470 nm and 525 nm. Spectra recording in minute intervals. Figure on formation of C30⁺ in Ref. 37.

exemplified for C30:9 (Fig. 5): rapid formation of ³C30 at 510 nm was observed, its fast decay, and the concurrent development of longer living C30⁺ at 815 nm. The spectra of all ³Car and Car⁺ are shown in Fig. 6. The peak heights of ³Car were similar, while those of Car⁺ increased with polyene chain length.

Kinetic measurements. Formation and decay of the transient species after flash photolysis (Scheme 2) are typified with C30:9.

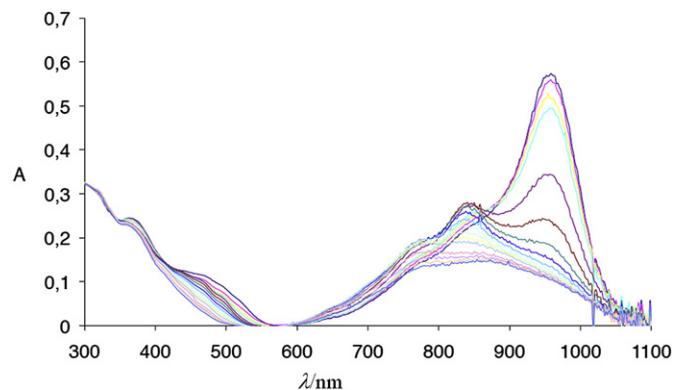


Fig. 4. Formation of C35⁺ (λ_{\max} =958 nm) with FeCl₃ in CH₂Cl₂. Secondary product at 845 nm. Spectra recording in minute intervals.

Table 1

Wavelength at maximum absorption (λ_{\max}) or 0 ← 0 vibrational transition of Car, and λ_{\max} of ³Car, and Car⁺ (photophysical generation=light, chemical formation=Fe); nd=not determined due to low compound amounts, decomposition, experimental or instrumental limitation

Car Cn	N	Car nm	³ Car nm	Car ⁺ (light) MeCN nm	Car ⁺ (Fe) CH ₂ Cl ₂ nm
20	5	360	434	573	568
22	6	388	455	642	633
25	7	416	466	714	725
27	8	440	485	763	765
30	9	464	502	821	850
32	10	484	nd	nd	891
35	11	503	535	920	958
40	13	525	557	nd	nd
45	15	539	586	nd	nd

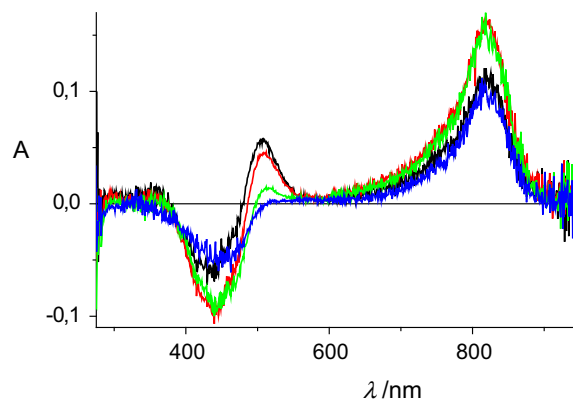


Fig. 5. Spectra of C30-transients in MeCN/H₂O 9:1 after irradiation of the Car/Rib solution at various delays (5 μs —, 15 μs —, 40 μs —, 80 μs —) between the irradiating pump flashes and the probe pulse. ³C30 λ_{\max} =510 nm, C30⁺ λ_{\max} =815 nm. The Rib transients were subtracted from the spectral traces of the compound mixture.

³Rib formed immediately after irradiation and was rapidly consumed by reaction with C30:9 to ³C30 and C30⁺. After 30 μs ³C30 had practically disappeared whereas the formation of C30⁺ had reached its maximum, then decaying in about 200 μs to unidentified products (Fig. 7).

The lifetime (20 min) of chemically produced C30⁺ was established by measuring the gradual decrease of its absorption (Fig. 8).³⁷ Car⁺ was sufficiently stable for detection by capillary electrophoresis; shorter chain Car⁺ migrated faster than longer chain Car⁺. The increased stability of the chemically generated Car⁺ may arise from concentration and solvent effects, or the presence of O₂ and counter ions.

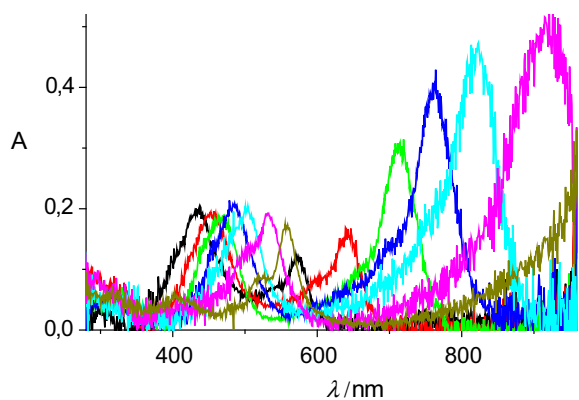


Fig. 6. ${}^3\text{Car}$ and Car^+ spectra (MeCN/H₂O=9:1) of C20 —, C22 —, C25 —, C27 —, C30 —, C35 — and C40 — recorded at a delay of 15 μs between the pump and the probe pulse. The intensity of the pump flashes and the concentrations of Rib and Cr were identical.

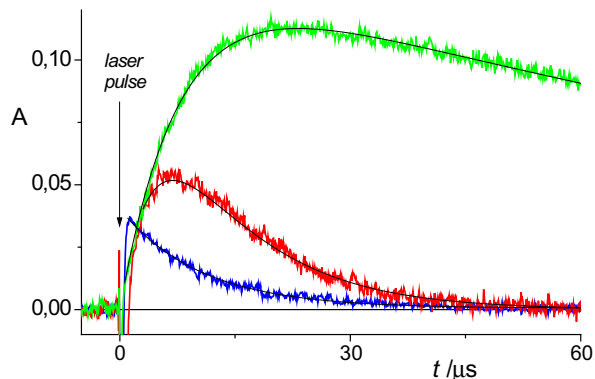


Fig. 7. Kinetic traces (average of absorbance vs time after 2 laser pulses into solutions of two different concentrations in MeCN/H₂O=9:1) for ${}^3\text{Rib}$ — at 680 nm, ${}^3\text{C30}$ — at 510 nm, and C30^+ — at 815 nm. The traces were fitted to the absorption graphs with a single exponential for ${}^3\text{Rib}$ and a double exponential for ${}^3\text{C30}$ and C30^+ .

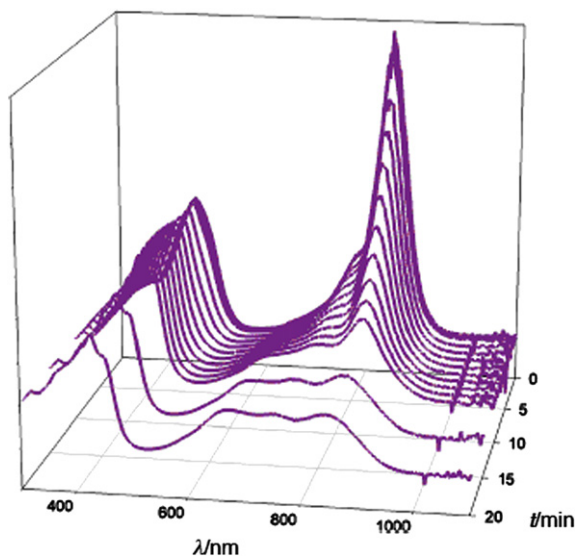


Fig. 8. Slow decay of C30^+ (from $\text{C30} + \text{FeCl}_3$ in CH_2Cl_2).

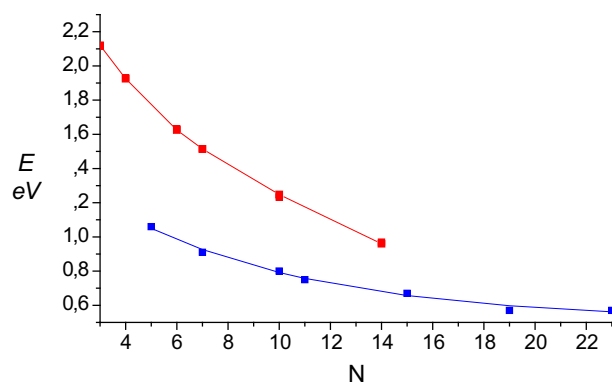


Fig. 9. Energetic relation between ${}^3\text{Car}$ — and redox potential $E(\text{Car}^+/\text{Car})$ — in relation to N .

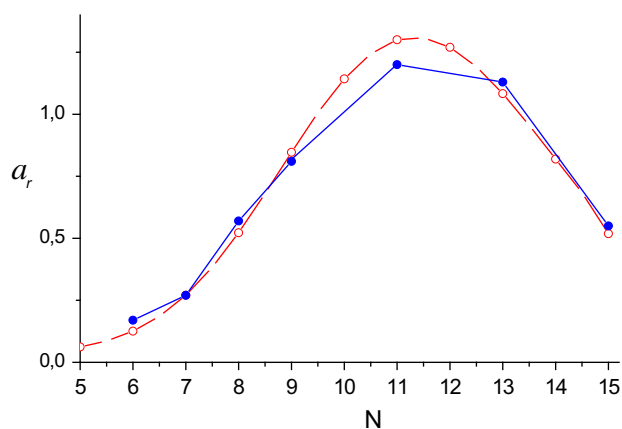


Fig. 10. Calculated — and experimental — antioxidant ratio a_r related to the number of double bonds N .

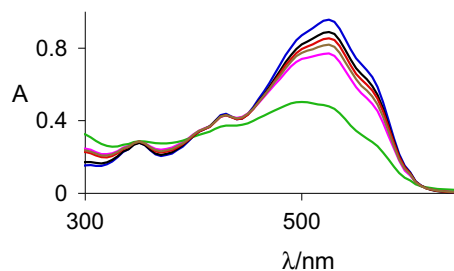


Fig. 11. Vis-spectra of C45-acid in benzene —, addition of I_2 —, radiation: 10 min —, 20 min —, 30 min —, 70 min —.

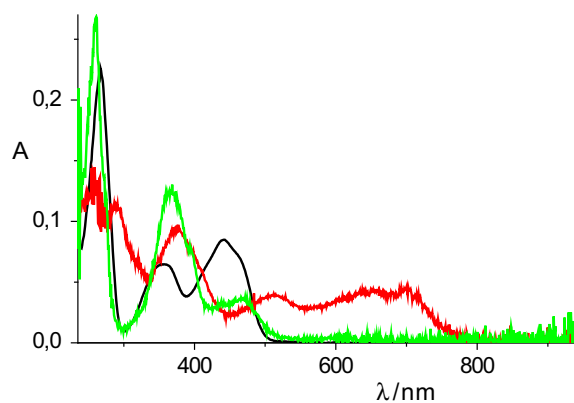
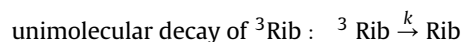


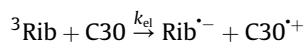
Fig. 12. Spectra of Rib (—), ${}^3\text{Rib}$ (—), and Rib^- (—).

2.1. Determination of the reaction constants, the antioxidant ratio a_r and the optimal chain length

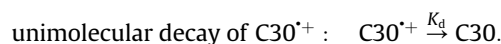
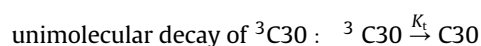
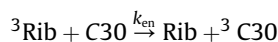
The reaction constants k_{el} and k_{en} (Scheme 2), exemplified for C30:9, were established from the sequences:



bimolecular decay by electron transfer :



bimolecular decay by energy transfer :



${}^3\text{Rib}$ decays exponentially in the presence of C30:9 with a quenching constant

$$K = (K_{en} + K_{el}) \cdot [\text{C30}] + k \quad (1)$$

Hence, the sum of electron and energy transfer reaction constants (k_{el} and k_{en}) can be found when the decay constant of ${}^3\text{Rib}$ is measured for different C30 concentrations (Table 2). The time-dependence of ${}^3\text{C30}$ decay was derived from

$$[{}^3\text{C30}(t)] = \frac{k_{en} \cdot [{}^3\text{Rib}_0] \cdot [\text{C30}]}{K_t - K} \cdot (e^{-K \cdot t} - e^{-K_t \cdot t}) \quad (2)$$

$$\equiv p \cdot (e^{-K \cdot t} - e^{-K_t \cdot t})$$

Based on this expression the kinetic trace for the absorbance of ${}^3\text{C30}$ was fitted to a difference of two exponentials multiplied by a parameter $P = \epsilon_T \cdot p$.

$$A({}^3\text{C30}(t)) = \epsilon_T \cdot [{}^3\text{C30}(t)] \cdot l = \epsilon_T \cdot p \cdot (e^{-K \cdot t} - e^{-K_t \cdot t}) \cdot l \quad (3)$$

(optical path length $l = 1$ cm)

The relation between P and k_{en} was set to

$$P = \frac{\epsilon_T \cdot k_{en} \cdot [{}^3\text{Rib}_0] \cdot [\text{C30}]}{K_t - K} \quad (4)$$

with

$$k_{en} = \frac{1}{\epsilon_T} \cdot \frac{P \cdot (K_t - K)}{[{}^3\text{Rib}] \cdot [\text{C30}]} = \frac{\epsilon_G}{\epsilon_T} \cdot \frac{P \cdot (K_t - K)}{[{}^3\text{Rib}] \cdot [A_{\text{C30}}]} \quad (5)$$

The energy transfer constant k_{en} resulted from the fitting routine, inserting the absorbance of C30 and the initial concentration of ${}^3\text{Rib}$, which was determined spectroscopically at 680 nm with the extinction coefficient $\epsilon = 6.0 \times 10^3 \text{ M}^{-1} \text{ cm}^{-1}$. The fitted kinetic traces are

Table 2

Quenching constant K , experimental reaction constants k_{el} and k_{en} , and experimental and calculated k_{el}/k_{en} ratio a_r

Car Cn	N	$K \text{ Rib} \cdot 10^9$	$k_{el} \text{ Car} \cdot 10^9$	$k_{en} \text{ Car} \cdot 10^9$	k_{el}/k_{en} exper.	k_{el}/k_{en} calcd
C22	6	2.5	0.41	2.4	0.17	0.13
C25	7	2.7	0.50	1.8	0.27	0.27
C27	8	3.9	0.75	1.3	0.57	0.52
C30	9	5.0	0.89	1.1	0.81	0.85
C35	11	10	1.20	0.9	1.33	1.14
C40	13	20	1.5	1.3	1.15	1.08
C45	15	26	1.07	2.5	0.42	0.42

seen in Fig. 7. The kinetic data of the other Car were calculated analogously. ${}^3\text{Rib}$ reacts faster with longer chain Car (increasing quenching constant K , Table 2); the various quenching constants K suggest diverse reaction processes depending on the number of double bonds. The constant k_{el} was determined similarly, taking into account the lifetime of $\text{Car}^{\bullet+}$. With k_{el} and k_{en} at hand the two major antioxidant mechanisms of Car (energy and electron transfer) could be summarized as antioxidant ratio $a_r = k_{el}/k_{en}$ (Table 2).

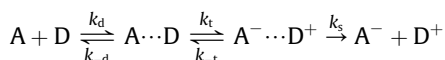
2.2. Theoretical calculation of the reaction constants, the antioxidant ratio a_r and the optimal chain length

Given that the transfer reactions in polyenes are diffusion-limited, the rate constant k_d was calculated with:

$$k_d = 4\pi \cdot R_{DA} \cdot (D_D + D_A) \cdot N_A \cdot 1000 \quad (6)$$

R_{DA} , the hydrodynamic radius of the $\text{Car}-{}^3\text{Rib}$ encounter complex, is the sum of the radii of the donor D and the acceptor A: $R_{DA} = R_D + R_A$. N_A is the Avogadro number and D represents the diffusion constant of the compound, which for a presumed spherical molecule of radius R is $D = k_B T / 6\pi R \eta$, where η stands for the viscosity of the solvent. Applying $R_D \approx 7.5 \text{ \AA}$ (Rib), $R_A \approx 2.5 \text{ \AA}$ (hydrodynamic radius of Car estimated from data given in Ref. 24) and $\eta_{\text{MeCN}} = 0.4 \times 10^{-3} \text{ N s/m}^2$ gave $k_d = 1.4 \times 10^{10} \text{ l/mol s}$.

The transfer reactions proceed in three steps: diffusion advances the dispersed molecules to proximity enabling electron or energy exchange forming tightly located products, which then separate:



The diffusion- and back diffusion-constants are denoted k_d and k_{-d} , the transfer- and back transfer rate constants k_t and k_{-t} , and the rate constant for product separation k_s .

Using the steady state approximation for intermediate concentrations, the formation rate F of charged species is expressed as:

$$F = (k_d/k_t + k_{-d}) \cdot (k_t/k_s + k_{-t}) \cdot k_s \approx k_d \quad (7)$$

When the rate constant for electron back transfer k_{-t} is small compared to the rate constant for separation k_s , and when the rate constant for back diffusion k_{-d} is smaller than that of transfer k_t , F is alike the rate constant k_d for a diffusion-limited reaction. Taking the transfer reactions into consideration F is expressed as:

$$F(\text{el}) = (k_{el}/k_{el} + k_{en}) \cdot k_d \quad (8)$$

and

$$F(\text{en}) = (k_{en}/(k_{el} + k_{en})) \cdot k_d \quad (9)$$

Mataga's Golden rule is applicable to non-adiabatic radiationless transitions with electronic interactions (V) smaller than $k_B T$, and with electron- or energy transfer in the weak coupling category ($V \ll k_B T$):⁴³

$$k_{\text{trans}} = \left(\frac{\pi}{\hbar^2 \cdot \lambda_s \cdot k_B T} \right)^{1/2} \cdot V^2 \sum_n \left(e^{-S} \left(\frac{S^n}{n!} \right) \right) \cdot \exp \left(- \frac{(\Delta G_0 + \lambda_s + n h \nu)^2}{4 \lambda_s k_B T} \right) \quad (10)$$

(k_{trans} =energy or electron transfer)

The solvent reorganization energy λ_s corresponds to the electrical work needed to reorganize the solvent molecules surrounding the two charged species in the electron transfer reaction; $S = \lambda_i / h \nu$ represents the inner reorganization energy, expressed as the crossing point of the vertical line from the minimum of the

reactant's energy parabola to the product parabola, ν is the averaged frequency for the nuclear motion in the parabolic potential energy surfaces, ΔG^0 denotes the free energy change, which for triplet energy transfer is

$$\Delta G^0 = E(^3\text{Car}) - E(^3\text{Rib}) \quad (11a)$$

$$\text{with } E(^3\text{Rib})=2.0 \text{ eV}^{44}$$

$$\Delta G^0 = E(^3\text{Car}) - 2.0 \text{ eV} \quad (11b)$$

The energetic relation between ^3Car and N was found with

$$E(^3\text{Car}) = 7.25 \left(1/N^{0.26} - 0.34 \cdot (1 + 1/N) \right) \text{ eV} \quad (12)$$

and reproduced the measured triplet levels as a function of N^{45} (Fig. 9).

When applying $V=0.024 \text{ eV}$, $\lambda_i=0.3 \text{ eV}$, $h\nu=0.15 \text{ eV}$, and $\lambda_s=0.40 \text{ eV}$ to Eq. 10 the energy transfer rates k_{en} were obtained. The electron transfer rate k_{el} was calculated from the Rehm–Weller equation for the free energy change in an electron transfer reaction:⁴⁶

$$\begin{aligned} \Delta G &= [E(\text{Car}^{*+}/\text{Car}) + f - E(\text{Rib}^{\cdot-}/\text{Rib})] - e^2/4\pi\epsilon \cdot r_{\text{DA}} + \lambda_s \\ &\quad - E(^3\text{Rib}) \\ &= [E(\text{Car}^{*+}/\text{Car}) + 0.24 \text{ eV} - (-0.3 \text{ eV})] - 0.7 \text{ eV} + 0.7 \text{ eV} \\ &\quad - 2.0 \text{ eV} \\ &= E(\text{Car}^{*+}/\text{Car}) - 1.46 \text{ eV}. \end{aligned} \quad (13)$$

The calculation was performed with values for redox potentials measured versus the standard hydrogen electrode (SHE): $E(\text{Rib}^{\cdot-}/\text{Rib})=-0.3 \text{ eV}$.⁴⁴ The Coulomb term is the electric energy gained from the two opposite charges e at distance r_{DA} , the distance of the closest approach of the electron donor Car and the acceptor Rib. In MeCN with a dielectric constant $\epsilon=37.5$ the Coulomb term is estimated 0.7 eV; the same value is taken for the reorganization energy λ_s . The redox potential $E(\text{Car}^{*+}/\text{Car})$ changes with N. Redox potentials have previously been evaluated with polyenes against the saturated calomel electrode.⁴⁷ Comparability was achieved by adding a factor $f=0.24 \text{ eV}$ to the SHE related values, which is the reference in the redox potential measurements of Rib. The found k_{el} -values were then divided by the rates of k_{en} ; the result is collected in Table 2.

For better comparison the previously obtained experimental data were reproduced by expressing redox potentials (Fig. 9):

$$E(\text{Car}^{*+}/\text{Car}) = 0.51 \text{ eV} + 0.70 \text{ eV} \cdot e^{-0.13N-3} \quad (14)$$

When the redox potential values were applied in Eq. 14, the resulting electron to energy transfers ratios were smaller by a factor of two compared with the experimental data. The deviation may originate from differences in λ_s for the individual Car. The shorter Car have a slightly larger λ_s than the longer chain Car, a linear relation between λ_s and the length of the molecule was assumed.

When the expression for ΔG was revised by inserting a term-modulating solvent reorganization energy

$$\Delta\lambda_s = -0.1(N - 7.5) \text{ eV} \quad (15)$$

a satisfactory agreement concerning the calculated and experimental transfer rates k_{el} and k_{en} was achieved (Fig. 10).

2.3. Comparison of experimental and calculated data

The calculated antioxidant ratio $a_r=k_{\text{el}}/k_{\text{en}}$ (Table 2) is in accordance with the experimentally determined a_r , both reaching the greatest magnitude with 11C=C bonds (Fig. 10). Our results with

Car support previous outcomes on optimal number of double bonds for other carotenoids. It is striking to note that carotenoids with 12 or 13 double bonds occur rarely, the longest natural carotenoid reaches 14C=C bonds.⁴⁸

3. Conclusion

Summarizing reactions, tables, and figures the following peculiarities were found: Carotenoic acids (Car) with 5–15 double bonds can both reduce triplet sensitizers and FeCl_3 . The spectroscopic nature of Car^{*+} , obtained by photophysical or chemical means, is identical. The two major antioxidant actions of carotenoids, electron, and energy transfer, sum up in a comprehensive expression, the antioxidant ratio $a_r=k_{\text{el}}/k_{\text{en}}$. Calculated and experimentally derived a_r of the investigated polyene acids series reached a maximum with 11 conjugated double bonds.

4. Experimental section

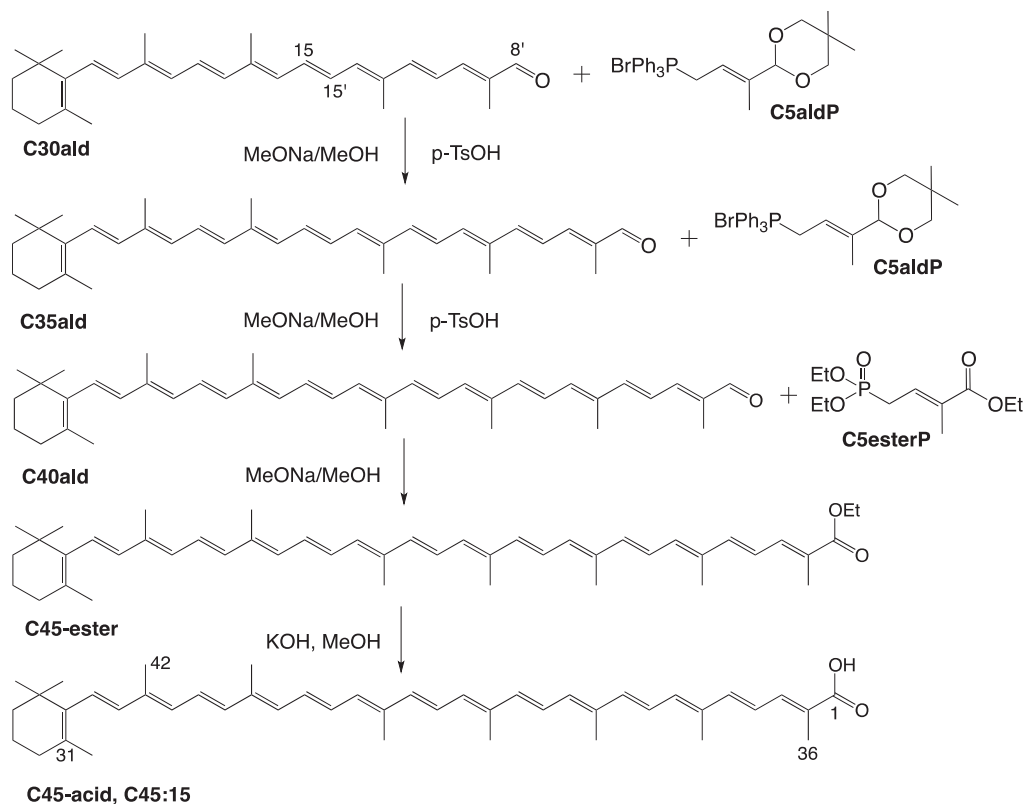
4.1. Synthesis

Acids C20:5–C35:15, C30-aldehyde (C30ald), the C5 Wittig salts C5aldP and C5esterP were produced by BASF.³⁸ C40- and C45-acid were synthesized by subsequent Wittig reactions⁴² from C30ald (Schemes 3 and 4) as exemplified for C45-acid: C30ald was reacted with the protected aldehyde Wittig salt C5aldP to C35-aldehyde (C35ald), which was extended with C5aldP to C40ald; which again was prolonged with C5esterP to C45-ester; hydrolysis afforded the acid C45:15.

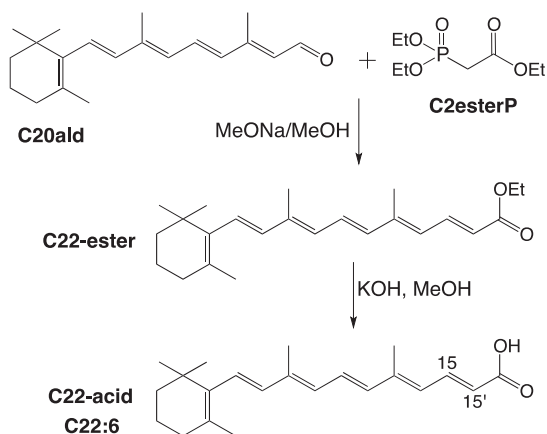
4.1.1. C35-aldehyde.⁴⁰ A solution of C30ald (0.2 g, 0.67 mmol) in dry MeOH (10 mL), phosphonium salt C5aldP (1.7 g, 3.4 mmol) in dry MeOH (20 mL), and MeONa (0.2 g, 3.4 mmol) in dry MeOH (10 mL) reacted at reflux temperature for 24 h. The solvent was removed and H_2O was added followed by repeated extraction of the aqueous phase with CH_2Cl_2 . The combined extracts were dried over MgSO_4 , the solvent was evaporated, the residue dissolved in acetone and *p*-toluenesulfonic acid (0.01 g) was added. After 2 h stirring the solvent was evaporated, H_2O was added, the mixture extracted with CH_2Cl_2 , and the combined extracts were dried over MgSO_4 . Flash chromatography (hexane/ethyl acetate, 3:1) of the residue gave C35ald (0.198 g, 85%). HRMS: calcd for $\text{C}_{35}\text{H}_{46}\text{O}$ 482.3549; found 482.3565.

4.1.2. C40-aldehyde (torularhodinaldehyde).⁴⁰ The aldehyde was synthesized analogously from C30ald (0.1 g, 0.21 mmol) in dry MeOH (10 mL), phosphonium salt C5aldP (1.0 g, 1.9 mmol) in dry MeOH (20 mL), and MeONa (0.1 g, 1.7 mmol) in dry MeOH (10 mL). Chromatography work-up afforded C40ald (60 mg, 53%). HRMS calcd for $\text{C}_{40}\text{H}_{52}\text{O}$ 548.4018; found 548.4015.

4.1.3. C45:15 acid. C40ald (23.5 mg, 0.043 mmol) in dry THF (20 mL) was reacted with C5esterP (74.5 mg, 0.145 mmol) in dry MeOH (20 mL) and MeONa (7.89 mg, 0.145 mmol) in dry MeOH (10 mL). The mixture was refluxed for 48 h and gave after work-up C45-ester, which was dissolved in methanol (30 mL). A solution of 25% KOH/MeOH (10 mL) was added and the mixture refluxed for 2 h.⁴⁹ The solvent was removed and the residue washed with 15% H_2SO_4 . The aqueous layer was extracted with CH_2Cl_2 and the combined organic phases were washed repeatedly with H_2O . Concentration under vacuum and purification by flash chromatography on silica gel (hexane/acetone 6:1) gave C45:15 (12 mg, 44%). ¹H NMR (400 MHz, DMSO-*d*₆): $\delta=1.07$ (s, 6H, 2CH₃, C35), 1.48 (m, 2H, C34), 1.60 (m, 2H, C33), 1.74 (s, 3H, CH₃, C31), 1.79 (s, 6H, 2CH₃, C23, C27), 1.87 (m, 12H, 4CH₃, in chain), 2.0 (m, 2H, C32), 2.05 (s, 3H, CH₃, C2), 6.16–7.26 (m, 21H, olefin protons), 12.24 (acid



Scheme 3.



Scheme 4.

corresponding aldehydes with Wittig salt C2esterP (representative synthesis in Scheme 4):



The acids C22, C25, C27, C35, and C40 have been previously synthesized by analogous syntheses.⁸

proton), for convenience the common carotenoid numbering has been abandoned (Scheme 3), IR: 1671 cm^{-1} , HRMS: calcd for $\text{C}_{45}\text{H}_{58}\text{O}_2$ 630.4433; found 630.4437.

4.1.4. C40:13 acid (torularhodin).⁴² The acid was synthesized analogously from C30ald with C5aldP followed by hydrolysis of the obtained C40:13 ester (8.4 mg, 75%). HRMS: calcd for $\text{C}_{40}\text{H}_{52}\text{O}_2$ 564.3967; found 564.3964. The NMR-data of the acids were comparable to the values given in Refs. 49 and 50.

4.1.5. Other acids. C25:7, C35:11, and C40:13 were synthesized similarly. C22:6, C27:8, and C32:11 were obtained from the

4.2. *cis/trans*-Isomers

The occurrence of *cis*-isomers, common for short chain polyenes, becomes unlikely with longer chain lengths (the longer the chain the more *trans*).^{51–53} The regular increase of λ_{max} with N supports the formation of all *trans*-isomers (Fig. 2, 2SD). The absence of spectral changes during the classical *cis*→*trans* isomerization experiment of C45:15 with I_2 and light was an additional indication for the predominance of the all-*trans* isomer: C45:15 was dissolved in benzene, a minute amount of I_2 in benzene was added and the solution exposed to bright sunshine; spectra were recorded until decomposition after 70 min (Fig. 11).^{54,55}

4.3. Chemical formation of Car⁺

A drop of a FeCl₃-solution (1.5% in CH₂Cl₂/acetone 50:1) was added to a cuvette filled with a carotenoic acid dissolved in CH₂Cl₂.³⁷ The formation of C20⁺, C22⁺, and C25⁺ was seen by an immediate color change; the absorption of longer chain Car⁺ occurred in the invisible wavelength range and the reaction solution appeared black. Capillary electrophoresis of C25⁺, C27⁺, C30⁺, and C32⁺ was performed by co-injection with the corresponding Car and acetophenone as neutral markers.³⁷ Since the charge was constant, shorter Car⁺ migrated faster than longer Car⁺.

4.4. Absorption extinction coefficient, oxidation potential

Absorption spectra were recorded using a Shimadzu UV-1601 PC spectrophotometer. The cuvettes with the Car-solutions were flushed with argon for 30 min and irradiated in an argon atmosphere. The relative error in determining ϵ , mostly due to the weighing, is less than 10%: $\epsilon \times 10^4$ [M⁻¹ cm⁻¹] C20:5 $\epsilon=4.97$, C22:6 $\epsilon=5.41$, C25:7 $\epsilon=6.87$, C27:8 $\epsilon=8.53$, C30:9 $\epsilon=10.20$, C32:10 $\epsilon=11.30$, C35:11 $\epsilon=11.90$. The calculated oxidation potentials of C20:5–C45:15 occur in the range $E_{ox}=1.2$ – 0.63 V (vs SHE).^{56,57}

4.5. Transient spectra

A miniaturized flash photolysis equipment, composed of commercial and purpose built units, was used. The pump beam (approximately 5 μ s) was generated by discharging a 2 μ F capacitor through a linear Xenon flash lamp (EG&G Model QXA 17) supplied with 3 kV. The discharge of the pump flash was monitored by a photomultiplier (PM) and the signal from the PM-tube was sent to a delay generator (Princeton Instruments, Model PG200). The output from the delay generator was triggering the probe lamp (EG&G Model FX-409U), which has a flash duration of 2 μ s. Both flashes were monitored by a storage oscilloscope (Le Croy 9410). The probe light is fixed at a right angle to the pump beam and is directed, after its emergence from the sample cuvette, by an optical fiber to an optical multichannel analyzer (Zeiss, MCS 224). The transient absorption spectrum was computed with a homemade software program: $A(t, \lambda i) = \lg[(Ri - Di/Si - Ei)]$ is the delay time between the pump and the probe flash set by the delay generator and measured by the storage oscilloscope. Di is the dark current in diode i , Ri is the intensity of the i th diode in the absence of pump flashes, and Si in the presence of a pump flash. Ei is the spectrum from the pump flashes only, and it contains essentially the resulting fluorescence spectrum of the substance; λi is the wavelength corresponding to diode number i .

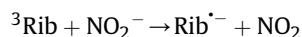
A transient absorption spectrum is defined as:

$$DA(l, t) = A(l, t) - A(l) = [e_p \cdot c_p \cdot l + e_g \cdot (c_0 - c_p) \cdot l] - e_g \cdot c_0 \cdot l \\ = (e_p - e_g) \cdot c_p \cdot l$$

where $A(\lambda, t)$ is the absorbance at time t after the pump flash, and $A(\lambda)$ is the absorbance before the flash. A certain concentration of photoproducts c_p is formed by the flash with extinction denoted ϵ_p , at the expense of ground state molecules. The extinction coefficients of the photoproduct and ground state molecules are denoted ϵ_p and ϵ_g , respectively, and the ground state concentration is c_0 . Inserting the fraction $a=c_p/c_0$ of the ground state absorption spectrum to the transient absorption spectrum allowed to obtain the spectrum of the photoproduct: $A_p(l, t) = DA(l, t) + a \cdot A(l) = e_p \cdot c \cdot l$.

The flash photolysis of the Rib/Car solution results in four species (Scheme 2, Fig. 12): Initially, the pump flash generates ³Rib; then the collision of ³Rib with Car forms Rib⁻, ³Car, and Car⁺. ³Rib and Rib⁻ spectra were acquired by exposing only Rib to pump flashes. Since the ground state depletion spectrum of irradiated Rib

(triplet minus singlet spectra, TmS-Rib) and the spectrum of ³Rib arise from similar concentrations, the extinction coefficient ϵ at λ_{max} of ³Rib was estimated in relation to the known extinction coefficient of Rib $\epsilon=1.10 \times 10^4$ M⁻¹ cm⁻¹ at 442 nm.⁵⁸ The ratio between the heights of the ³Rib absorption at 700 nm and the Rib absorption at 442 nm is 0.50 and hence $\epsilon \approx 0.55 \times 10^4$ M⁻¹ cm⁻¹ for ³Rib. These ϵ -values were needed in the calculation of the rate constants k_{el} and k_{en} . The Rib⁻ spectrum was verified after adding NO₂⁻ to the Rib-solution. Irradiation formed ³Rib, which immediately reacted to Rib⁻ by an electron transfer reaction:



As all ³Rib was converted with NO₂⁻ to Rib⁻ its ϵ was derived analogously to the calculation of ³Rib.

³C30 and C30⁺ were acquired by subtraction of the ³Rib and Rib⁺ spectra (TmS-Rib and DmS-Rib; Singlet S, doublet D and triplet T designate the eigenstates adopted by the electron spin of the molecule) from the spectral traces of the mixture at various delays between the irradiating pump flashes and the probe pulse (Fig. 5). The ³C30 absorption corresponds to the difference spectrum recorded after 15–40 μ s, while the C30⁺ spectrum is almost identical to the absorption after 80 μ s. The ϵ -ratio ³C30/C30 is 1.5 with the corresponding ratio C30⁺/C30=1.8. These ratios were virtually identical to the other ³Car and Car⁺, were, therefore, likewise attributed to ³C32, C32⁺, C40⁺, and C45⁺ (λ_{max} not detectable, Table 1, Fig. 6), and were used for calculating k_{el} and k_{en} .

The comparison of the ³Car and Car⁺ spectra in Fig. 6 was possible using similar intensities of the pump beams and equal concentrations of Rib. Since the reactions in Scheme 2 are bimolecular, the rate of formation depends upon the product of ³Rib and Car concentrations; therefore, small variations in quantities of Car were adjusted.

ΔE (eV) of Car (S₀→S₂), ³Car (T→T) and Car⁺ (D→D) were calculated from λ_{max} for C20–C27 and from the 0←0 vibrational transitions for C30–C45. When E is plotted against the inverse number of double bonds 1/N the slopes (B factor) of the linear graphs for Car and Car⁺ ($\Delta E=A+B/N$) were found similar (Fig. 2SD).

4.6. Kinetic measurements

The time-dependence of the signal $DA(l, t)$ at a fixed wavelength was recorded in a kinetic spectrometer, in which the pump source was the third harmonic of a pulsed Nd:YAG laser (BM Industries); a 150 W tungsten-halogen lamp provided the monitoring light, and a prism monochromator (Zeiss M4 QIII), placed behind the sample compartment, served as the wavelength selector. The pump and probe beams were perpendicular to each other. A Hamamatsu photomultiplier (R928) with a 50- Ω terminating resistor was used for detecting the light emerging from the exit slit of the monochromator, and the output of the detector was recorded by a 600 MHz digital storage oscilloscope (Agilent, Infinium 54830B). The transients shown here are averages of two recordings.

Formation and decay of the C20–C45 transients are typified with C30. C30⁺ appeared at 815 nm, the main contribution at 680 nm to the overall absorbance (A) is caused by ³Rib, at 510 nm both ³C30 and ³Rib were absorbing (Figs. 6 and 12). The absorbance of the transients were determined by:

$$A(\text{C30}^+(815)) = A(815) - \alpha \cdot A(680)$$

$$A(\text{Rib}(680)) = A(680) - \beta \cdot A(\text{C30}^+(815))$$

$$A(\text{C30}(510)) = A(510) - \gamma \cdot A(\text{Rib}(680))$$

Factor α is the fraction of the TmS-Rib spectrum at 815 nm relative to that at 680 nm ($\alpha=0.08$); similarly, β is the fraction of the DmS-Car spectrum at 680 nm relative to 815 nm ($\beta=0.14$) and γ is the fraction of the TmS-Rib spectrum at 510 nm relative to 680 nm ($\gamma=0.76$). This procedure allowed the plotting of the kinetic traces for ^3Rib , $^3\text{C30}$, and C30^+ demonstrating the varying lifetime of the species (Fig. 7).

Acknowledgements

We thank Dr. S.V. Gonzales for recording the HRMS spectra of C40:13 and C45:15.

Supplementary data

Supplementary data related to this article can be found at <http://dx.doi.org/10.1016/j.tet.2012.10.041>.

References and notes

- Edge, R.; Truscott, T. G. In *The Photochemistry of Carotenoids*; Frank, A. A., Young, A. J., Britton, G., Cogdell, R. J., Eds.; Kluwer: New York, NY, 1999.
- Fiedor, J.; Fiedor, L.; Haessner, R.; Scheer, H. *Biochim. Biophys. Acta* **2005**, *1709*, 1–4.
- Galano, A.; Vargas, R.; Martinez, A. *Phys. Chem. Chem. Phys.* **2010**, *12*, 193–200.
- El-Agamey, A.; Lowe, G. M.; McGarvey, D. J.; Mortensen, A.; Phillip, D. M.; Truscott, T. G.; Young, A. J. *Arch. Biochem. Biophys.* **2004**, *430*, 37–48.
- Xiang, J. F.; Rondonuwu, F. S.; Kakitani, Y.; Fujii, R.; Watanabe, Y.; Koyama, Y.; Nagae, H.; Yamano, Y.; Ito, M. *J. Phys. Chem. B* **2005**, *109*, 17066–17077.
- Martin, H. D.; Kock, S.; Scherrers, R.; Lutter, K.; Wagener, T.; Hundsdörfer, C.; Frixel, S.; Schaper, K.; Ernst, H.; Schrader, W.; Görner, H.; Stahl, W. *Angew. Chem., Int. Ed.* **2009**, *48*, 400–403.
- Lockwood, S. F.; Gross, G. J. *Cardiovasc. Drug Rev.* **2005**, *23*, 199–216.
- Wang, X. F.; Fujii, R.; Ito, S.; Koyama, Y.; Yamano, Y.; Ito, M.; Kitamura, T.; Yanagida, S. *Chem. Phys. Lett.* **2005**, *416*, 1–6.
- Akahane, J.; Rondonuwu, F. S.; Fiedor, L.; Watanabe, Y.; Koyama, Y. *Chem. Phys. Lett.* **2004**, *393*, 184–191.
- Ritz, T.; Damjanovic, A.; Schulten, K.; Zhang, J. P.; Koyama, Y. *Photosynth. Res.* **2000**, *66*, 125–144.
- Farhoosh, R.; Chynwat, V.; Gebhard, R.; Lugtenburg, J.; Frank, H. A. *Photochem. Photobiol.* **1997**, *66*, 97–104.
- Claes, H. *Biochem. Biophys. Res. Commun.* **1960**, *3*, 585–590.
- Foote, C. S.; Chang, Y. C.; Denny, R. W. *J. Am. Chem. Soc.* **1970**, *92*, 5216–5218.
- Krinsky, N. I. In *Carotenoids*; Isler, O., Ed.; Birkhäuser: Basel, 1971; pp 676–678.
- Rice-Evans, C. A. *Free Radical Res.* **2000**, *33*, S59–S66.
- Young, I. S. *J. Clin. Pathol.* **2001**, *54*, 334–339.
- Lissi, E.; Salimhanna, M.; Pascual, C.; Delcastillo, M. D. *Free Radical Biol. Med.* **1995**, *18*, 153–158.
- Huang, D. J.; Ou, B. X.; Prior, R. L. *J. Agric. Food Chem.* **2005**, *53*, 1841–1856.
- Baltschun, D.; Beutner, S.; Briviba, K.; Martin, H. D.; Paust, J.; Peters, M.; Rover, S.; Sies, H.; Stahl, W.; Steigel, A.; Stenhorst, F. *Liebigs Ann./Recl.* **1997**, 1887–1893.
- Sliwka, H. R.; Melø, T. B.; Foss, B. J.; Abdel-Hafez, S. H.; Partali, V.; Nadolski, G.; Jackson, H.; Lockwood, S. E. *Chem.—Eur. J.* **2007**, *13*, 4458–4466.
- Mohamad, S. B. B.; Yousef, Y. A.; Melø, T. B.; Javorfi, T.; Partali, V.; Sliwka, H. R.; Naqvi, K. R. *J. Photochem. Photobiol., B* **2006**, *84*, 135–140.
- Karagiannidou, E.; Størseth, T. R.; Sliwka, H. R.; Partali, V.; Malterud, K. E.; Tsimidou, M. *Eur. J. Lipid Sci. Technol.* **2003**, *105*, 419–426.
- Yanishlieva, N. V.; Marinova, E. M.; Raneva, V. G.; Partali, V.; Sliwka, H. R. *J. Am. Oil Chem. Soc.* **2001**, *78*, 641–644.
- Foss, B. J.; Sliwka, H. R.; Partali, V.; Cardounel, A. J.; Zweier, J. L.; Lockwood, S. F. *Bioorg. Med. Chem. Lett.* **2004**, *14*, 2807–2812.
- Naalsund, T.; Malterud, K. E.; Partali, V.; Sliwka, H. R. *Chem. Phys. Lipids* **2001**, *112*, 59–65.
- Sun, Y. J.; Pang-jie, Ye, X. Q.; Lu-Yuan; Li-Jun. *Chin. J. Struct. Chem.* **2009**, *28*, 163–170.
- Kleinová, M.; Hewitt, M.; Brezová, V.; Madden, J. C.; Cronin, M. T. D.; Valko, M. *Gen. Physiol. Biophys.* **2007**, *26*, 97–103.
- Pogson, B. J.; Rissler, H. M.; Frank, H. A. *Adv. Photosynth. Respir.* **2005**, *22*, 515–537.
- Naqvi, K. R.; Melø, T. B.; Sliwka, H. R.; Mohamad, S. B. B.; Partali, V. *Photochem. Photobiol. Sci.* **2003**, *2*, 381–385.
- Ramamurthy, V.; Liu, R. S. H. *J. Am. Chem. Soc.* **1976**, *98*, 2935–2942.
- Tinkler, J. H.; Tavender, S. M.; Parker, A. W.; McGarvey, D. J.; Mulroy, L.; Truscott, T. G. *J. Am. Chem. Soc.* **1996**, *118*, 1756–1761.
- Becker, R. S.; Bensasson, R. V.; Lafferty, J.; Truscott, T. G.; Land, E. J. *J. Chem. Soc., Faraday Trans. 2* **1978**, *74*, 2246–2255.
- Naqvi, K. R.; Melø, T. B.; Javorfi, T.; Gonzalez-Perez, S.; Arellano, J. B. *Phys. Chem. Chem. Phys.* **2009**, *11*, 6401–6405.
- Gao, Y. L.; Shinopoulos, K. E.; Tracwell, C. A.; Focsan, A. L.; Brudvig, G. W.; Kispert, L. D. *J. Phys. Chem. B* **2009**, *113*, 9901–9908.
- Kispert, L. D.; Konovalova, T.; Gao, Y. *Arch. Biochem. Biophys.* **2004**, *430*, 49–60.
- Lafferty, J.; Roach, A. C.; Sinclair, R. S.; Truscott, T. G.; Land, E. J. *J. Chem. Soc., Faraday Trans. 1* **1977**, *73*, 416–429.
- Li, H.; Rebmann, E.; Øpstad, C. L.; Schmid, R.; Sliwka, H. R.; Partali, V. *Eur. J. Org. Chem.* **2010**, 4630–4636.
- Krause, W.; Münster, P.; Ernst, H.; Paust, J.; Schulz, B.; Kochner, A.; Etzrodt, H. DE19506999, BASF SE, 1996.
- Karrer, P.; Eugster, C. H. *Helv. Chim. Acta* **1951**, *34*, 1805–1814.
- Schwieter, U.; Gutmann, H.; Lindlar, H.; Marbet, R.; Rigassi, N.; Rüeegg, R.; Schaeren, S. F.; Isler, O. *Helv. Chim. Acta* **1966**, *49*, 369–390.
- Andersson, P. O.; Gillbro, T. *J. Chem. Phys.* **1995**, *103*, 2509–2519.
- Isler, O.; Guex, W.; Rüeegg, R.; Ryser, G.; Saucy, G.; Schwieter, U.; Walter, M.; Winterstein, A. *Helv. Chim. Acta* **1959**, *42*, 864–871.
- Mataga, N.; Chosrowjan, H.; Shibata, Y.; Yoshida, N.; Osuka, A.; Kikuzawa, T.; Okada, T. *J. Am. Chem. Soc.* **2001**, *123*, 12422–12423.
- Lu, C. Y.; Wang, W. F.; Lin, W. Z.; Han, Z. H.; Yao, S. D.; Lin, N. Y. *J. Photochem. Photobiol., B* **1999**, *52*, 111–116.
- Kurashige, Y.; Nakano, H.; Nakao, Y.; Hirao, K. *Chem. Phys. Lett.* **2004**, *400*, 425–429.
- Fournier, T.; Tavender, S. M.; Parker, A. W.; Scholes, G. D.; Phillips, D. J. *Phys. Chem. A* **1997**, *101*, 5320–5326.
- Heinze, J.; Tschuncky, P.; Smie, A. *J. Solid State Electrochem.* **1998**, *2*, 102–109.
- Kushwaha, S. C.; Gochnauer, M. B.; Kushner, D. J.; Kates, M. *Can. J. Microbiol.* **1974**, *20*, 241–245.
- Larsen, E.; Abendroth, J.; Partali, V.; Schulz, B.; Sliwka, H. R.; Quartey, E. G. K. *Chem.—Eur. J.* **1998**, *4*, 113–117.
- Englert, G. In *Carotenoids*; Britton, G., Liaaen-Jensen, S., Pfander, Eds.; Spectroscopy; Birkhäuser: Basel, 1995; Vol. 1B.
- Kuhn, R.; Winterstein, A. *Helv. Chim. Acta* **1928**, *11*, 87–116.
- Koyama, Y.; Fujii, R. In *The Photochemistry of Carotenoids*; Frank, H. A., Young, A. J., Britton, G., Cogdell, R. J., Eds.; Kluwer: Dordrecht, 1999; p 172.
- Christensen, R. L.; Barney, E. A.; Broene, R. D.; Galinato, M. G. I.; Frank, H. A. *Arch. Biochem. Biophys.* **2004**, *430*, 30–36.
- Kon, M.; Britton, G. *Food Sci. Technol. Res.* **1999**, *5*, 347–349.
- Hepperle, S. S.; Li, Q. B.; East, A. L. *J. Phys. Chem. A* **2005**, *109*, 10975–10981.
- Bobrowski, K.; Das, P. K. *J. Phys. Chem.* **1986**, *90*, 927–931.
- Fungo, F.; Otero, L.; Durantini, E.; Thompson, W. J.; Silber, J. J.; Moore, T. A.; Moore, A. L.; Gust, D.; Sereno, L. *Phys. Chem. Chem. Phys.* **2003**, *5*, 469–475.
- Heelis, P. F.; Phillips, G. O. *Photobiochem. Photobiophys.* **1979**, *1*, 63–70.